

## P1.1 AIR-SEA INTERACTION PROCESSES IN WARM AND COLD SECTORS OF EXTRATROPICAL CYCLONIC STORMS OBSERVED DURING FASTEX

P. Ola G. Persson<sup>1</sup>, J. E. Hare<sup>1</sup>, C. W. Fairall<sup>2</sup>, and W. Otto<sup>2</sup>

<sup>1</sup>CIRES/NOAA/ETL, Boulder, CO

<sup>2</sup>NOAA/ETL, Boulder, CO

### 1. INTRODUCTION

During the Fronts and Atlantic Storm Tracks Experiment (FASTEX) (Joly et al. 1999), extensive measurements of the atmospheric boundary layer structure, air-sea interaction processes, and ocean surface were obtained from four ships strategically placed in the central North Atlantic Ocean during January and February 1997. Ten to twenty storm systems passed each ship, with surface winds of 15-30 ms<sup>-1</sup> associated with each passage. This data set allows us to examine how air-sea interaction processes are modulated by the storms and how these processes in turn impact the structures important for the development of these storm systems, especially the dynamically important warm sector region. In addition, the data also suggest how well satellite-based measurements, which rely on some of these air-sea interaction processes, can determine basic near-surface atmospheric parameters in specific regions of the storms.

In this paper, we will utilize the ship measurements to examine the surface-layer processes occurring in the warm sector and post-frontal regimes of the extratropical cyclones encountered in the North Atlantic. The presentation will focus on the data from the *R/V Knorr*, though data from the other ships have also been examined. A method for compositing the data has been designed. This compositing method allows us to locate the processes relative to the surface cold front, the warm sector, or the post-frontal sector.

### 2. METHOD

#### 2.1 Available Data

For measuring fluxes of momentum, sensible heat and latent heat using both the covariance and the dissipation methods, instrumentation on board the *R/V Knorr* included a Gill sonic anemometer using strapdown navigation to compensate for mast motions and an Ophir IR hygrometer (Fairall et al. 1997), a floating sea-surface temperature thermistor, and standard bulk meteorological measurements, including ship-

intake sea-surface temperatures.

Wave-height spectra, necessary for interpretation of the surface fluxes, were objectively provided by a TSK wave-height recorder on loan from Bedford Institute of Oceanography (BIO). Subjective estimates of sea-surface conditions, swell heights, and wave directions were provided by the ship crew from the bridge at least once every 4 hours.

Supplementary data collected on the *R/V Knorr* were used in the analysis but are not explicitly presented. These include winds up to 3-6 km from a NCAR 915-MHz ship-mounted wind profiler, cloud base and PBL height from a vertically pointing aerosol/cloudbase lidar, soundings at least every 6 hours [every 1.5-3 hours during intensive observation periods (IOPs)] from a NCAR OMEGA rawinsonde system, fluxes of downwelling longwave and shortwave radiation; cloud and precipitation structure from an extra-sensitive, vertically pointing, Doppler S-band radar, precipitation using an NCAR optical raingauge and a University of Kiel ship raingauge, and videotapes of the sea-state.

The flux instruments were mounted on a pivoting 20-m bow mast designed to allow maintenance access from an upper deck. Periodic cleaning of salt from the Ophir hygrometer was accomplished through a mast-mounted hose system. The sonic anemometer and Ophir data were rigorously edited to ensure data quality.

#### 2.2 Compositing Method

In order to place the observations in a storm-relative framework, the start of the warm sector, the surface cold-frontal passage, and the end of the post-frontal sector were defined from basic meteorological parameters. The near-surface specific humidity was used as a key parameter to define the onset of the warm-sector region and the end of the post-frontal region. The surface increase of specific humidity at the onset of the warm-sector region and the disappearance of the humidity perturbation at the end of the post-frontal region were clear in every case (e.g., Fig. 1a). The cold-frontal passage was defined by the surface wind shift (Fig. 1a). Therefore, the warm sector region is defined as the time between the

---

Corresponding author: Dr. Ola Persson, CIRES/NOAA/ETL, R/ET7, 325 Broadway, Boulder, CO 80305. email: ola.persson@noaa.gov

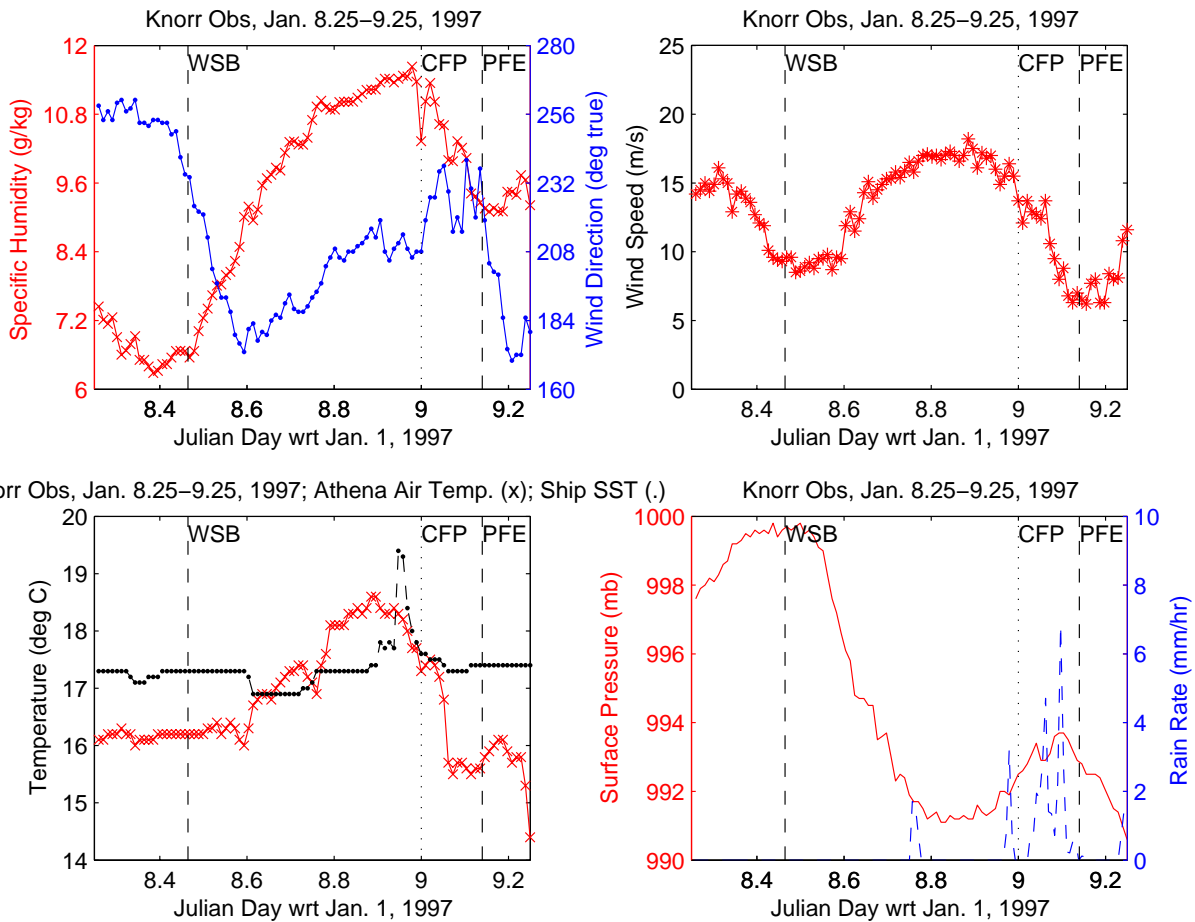


Fig. 1: Time series of a) specific humidity (x) and wind direction (dot), b) 18-m wind speed, c) sea surface (dot) and air (x) temperatures, and d) surface pressure (solid) and rain rate (dashed) for case 4 (JD8.25-9.25).

increase in the surface specific humidity and the wind shift, while the post-frontal regime is defined as the period between the wind shift and the end of the decrease in specific humidity. Typical changes in air temperature, wind speed, surface pressure, and precipitation were often seen, though these weren't used to define the transitions.

Table 1 shows the ten cases used for the *R/V Knorr*. The duration of the warm sector averaged 17.5 hours, ranging from 3.1- 43.4 hours. The post-frontal region was less than half that in duration. The first seven cases were obtained south and east of the Gulf Stream sea-surface temperature front, while the last three cases were obtained in the colder waters to the north and west of this front.

The storms' movements past each ship produced a northeast-to-southwest "track" for each ship through each storm (Fig. 2). The orientation and path of the storm determined the obliqueness of the ships' tracks. For example, the tracks were

nearly orthogonal to the surface cold front in cases 3 and 6, while they were nearly parallel for cases 4 and 8. With these definitions, statistical composites of storm-relative atmospheric parameters, surface fluxes, and wave characteristics were computed for each ship. The composites were temporally normalized using the duration of the warm sector region for each case. Hence the warm sector occurs for a normalized time of -1 - 0 and the post-frontal sector for a normalized time of 0 - 1. The difference in duration between the post-frontal region and the warm sector led to few samples during the latter half of the normalized post-frontal region.

### 3. SURFACE LAYER DESCRIPTION

#### 3.1 Atmospheric

The composites of the basic surface layer parameters of air temperature, specific humidity, wind speed and wind direction show regular variations relative to the location of the surface front (Fig. 3). The air temperature shows an

Table 1: Characteristics of the FASTEX cases used for compositing the R/V Knorr data.

Case	Warm sector duration (hr)	Cold-frontal passage (decimal JD)	Post-frontal sector duration (hr)	System phase velocity ( $\text{m s}^{-1}/\text{deg}$ )	15-min, 18 m LLJ wind speed max ( $\text{m s}^{-1}$ )	Avg. SST (deg C)
1	16.44	4.885	3.48	18.4/210	21.5	15.0
2	3.12	5.190	15.84	11.6/225	19.1	15.4
3	18.62	7.776	6.58	18.7/254	19.6	17.4
4	12.84	9.0	3.36	33.4/240	19.0	17.4
5	3.50	9.425	2.76	26.4/233	21.3	17.3
6	7.92	12.99	4.80	25.0/258	18.6	15.4
7	43.44	20.21	16.08	23.2/229	20.0	14.5
8	15.36	22.05	13.20	27.4/234	18.3	3.4
9	28.32	24.08	12.48	25.7/266	18.0	4.0
10	25.68	26.37	5.52	27.3/234	22.0	3.2
Average	17.5	N/A	8.4	23.7/238	19.7	16.1/3.5*

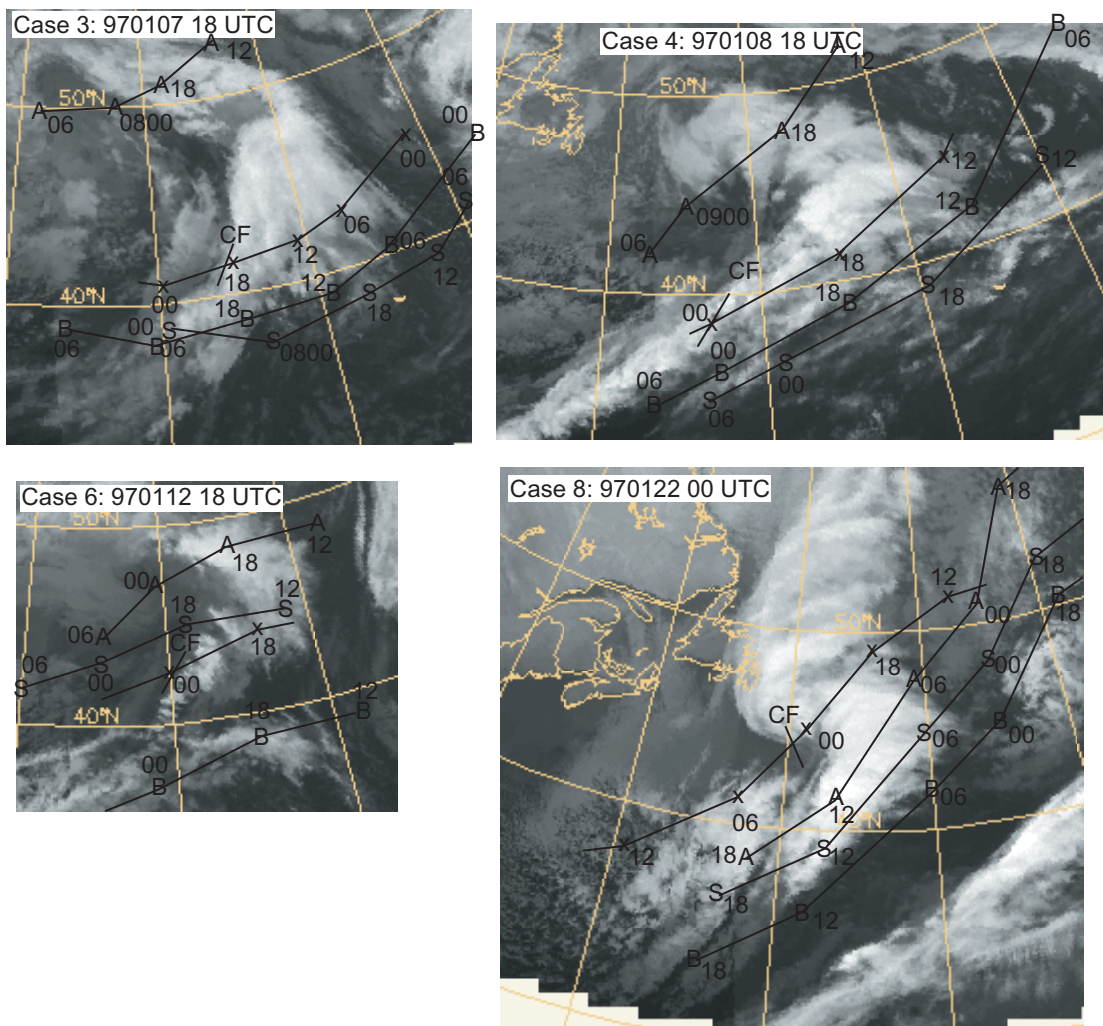


Fig. 2: Time-to-space converted tracks of the research vessels Knorr (x), Aegir (A), Victor Bugaev (B), and Suroit (S) through cases 3, 4, 6 and 8. The overlaid infrared satellite image corresponds to a time shortly prior to when the R/V Knorr passed through the surface cold front. The times next to each symbol marks the hour at that location.

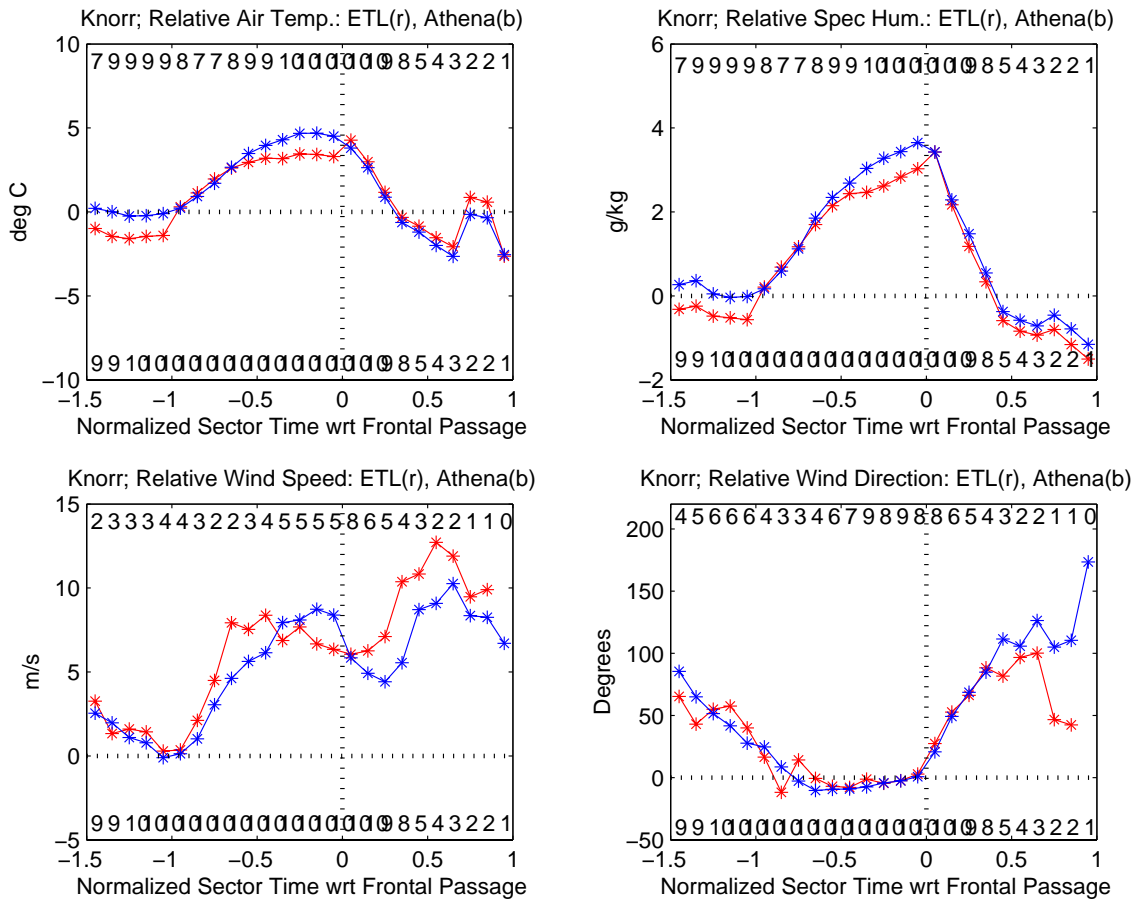


Fig. 3: Composite relative values of a) temperature, b) specific humidity, c) wind speed, and d) wind direction. Values are relative to their values at the onset of the warm sector, except for wind direction, which is relative to the value 1 hour before frontal passage. The numbers along the top and bottom of each frame shows the number of cases that contributed to each composite bin for each of the two sets of instrumentation available on the R/V Knorr.

increase of about  $4^{\circ}\text{C}$  from the onset of the warm sector to just before the cold frontal passage, dropping behind the cold front. The specific humidity increases nearly  $4\text{ g kg}^{-1}$  within the warm sector, peaking just before the cold-frontal passage. The wind speed shows the surface-layer manifestation of the classical low-level jet shortly before frontal passage, with an increase of about  $8.5\text{ m s}^{-1}$  from the onset of the warm sector. The maximum composite wind speed was about  $17\text{ m s}^{-1}$  in the warm sector, though the maximum 15-min 20-m wind speeds during the warm sector averaged  $19.7\text{ m s}^{-1}$ , and ranged from  $18\text{--}22\text{ m s}^{-1}$  (Table 1). The wind speed initially drops at the cold frontal passage, but then increases to another peak in the post-frontal region. In the transit from the eastern edge of the warm sector, the wind direction initially has a more westerly component than at the cold frontal passage, and then a slightly more easterly component. This implies

that the surface-layer flow is diffluent at the eastern edge of the warm sector, and then becomes confluent near the middle of the warm sector. Note that the onset of the wind speed increase occurs west of the eastern edge of the warm sector, as defined by the specific humidity. Hence, the thermodynamic and kinematic definitions of the warm sector region aren't exactly coincident.

### 3.2 Oceanic

The significant wave heights (the mean of the highest one-third wave heights) increased from about  $2.3\text{ m}$  in the eastern half of the warm sector to about  $3.9\text{ m}$  at the time of frontal passage (Fig. 4a). The maximum wave heights were about  $5.5\text{ m}$  in the eastern half of the warm sector increasing to about  $9\text{ m}$  at the time of frontal passage. The period of the significant waves was at a minimum of  $6.5\text{ s}$  within the eastern half of the warm sector,

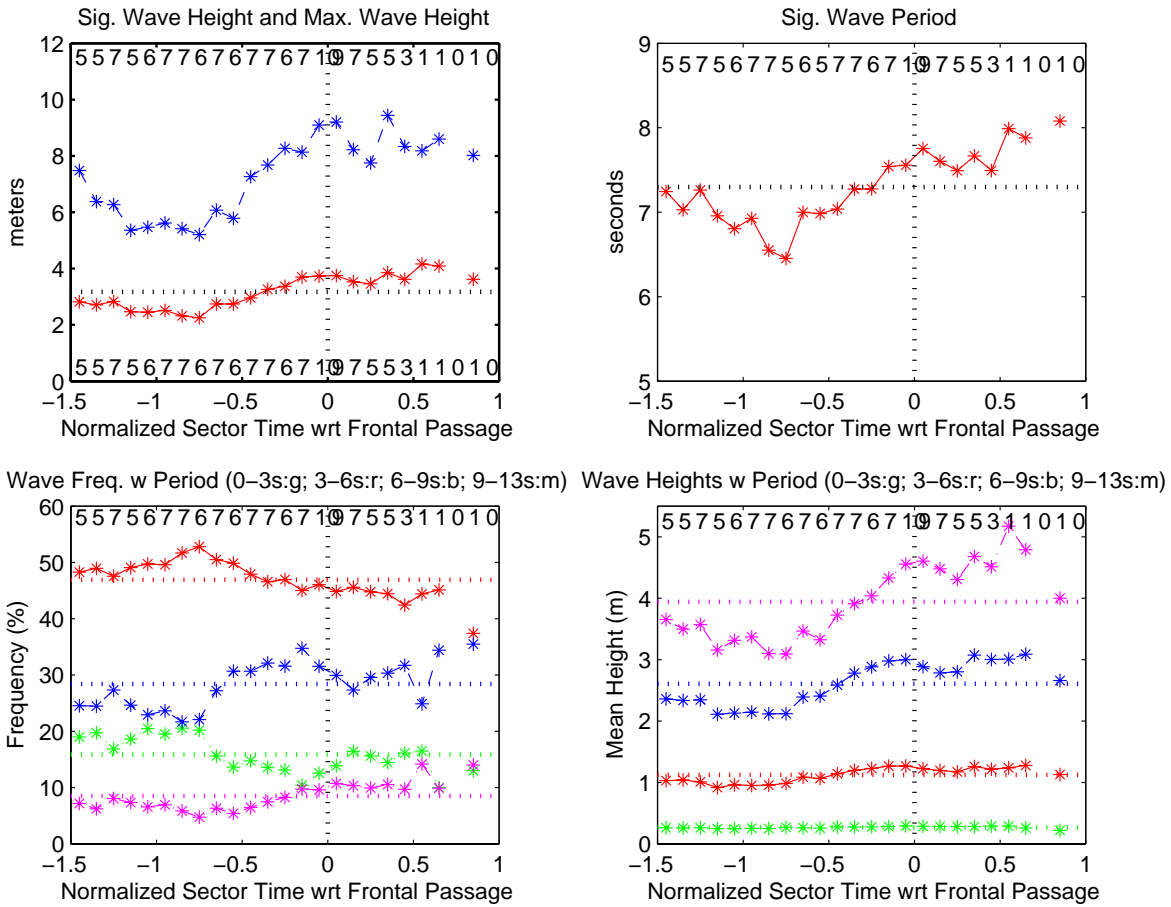


Fig. 4: Composite values of a) significant (red) and maximum (blue) wave heights, b) significant wave period, c) wave frequency for different wave period bins, and d) wave height for different wave period bins. The wave period bins in c) and d) are 0-3 s (green), 3-6 s, (red), 6-9 s (blue), and 9-12 s (magenta).

and reached a maximum of 7.8 - 8.0 s shortly after frontal passage (Fig. 4b). Hence, wave growth and an increase of the wave period occurs within the warm sector to just after the cold frontal passage. Note that the changes in wave height and period doesn't occur until after the onset of the increase in the wind speed, which occurs after the ship has been in the warm sector for 2-3 hours.

By splitting the wave data into wave period bins, we find the following: 1) the frequency of occurrence of waves with periods > 6 s increases in the last two-thirds of the warm sector at the expense of the waves with periods < 6 s (Fig. 4c), and 2) the mean height of the waves with periods > 3 s increase in the warm sector (Fig. 4d). Note that the response in the wave height occurs first for the short period waves. This is consistent with the one case shown by Rieder and Smith (1998).

#### 4. SURFACE FLUXES

Turbulent fluxes were determined through the covariance technique, the inertial dissipation technique, and the bulk formulas of Fairall et al (2002). The covariance values show the increase of stress beginning at a normalized time of about -0.75, at about the time the wind speed increases and the wave characteristics respond (Fig. 5a). The peak stress of  $0.7 \text{ N m}^{-2}$  occurs a little before the cold frontal passage at the time of maximum surface layer wind speed, peak in the occurrence of the 6-9 s period waves and near the peak in heights of these waves. Comparably high values of stress also occur in the post-frontal regime.

The sensible heat flux ( $H_s$ ) is a maximum in the post-frontal regime and before the onset of the warm sector (Fig. 5b). Within the warm sector,  $H_s$  decreases as the front approaches the ship, becoming slightly negative just before the passage of the surface cold front. Qualitatively, this is consistent with the warming of the prefrontal air

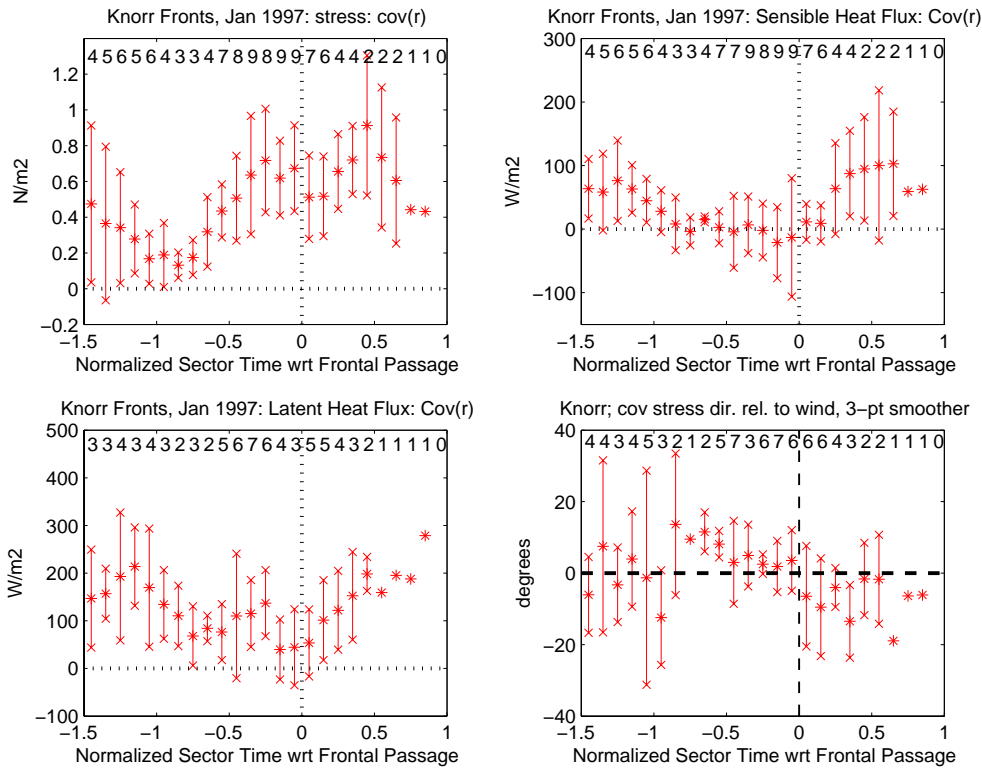


Fig. 5: Composite values of a) stress, b) sensible heat flux, and c) latent heat flux determined from the covariance method. Panel d) shows the composite of the difference between the stress direction and wind direction. A 3-point running mean was applied to the stress components before the stress direction was calculated. The vertical errors bars show  $\pm$  one standard deviation.

through horizontal advection and surface-layer fluxes producing a stable environment nearest the front and hence negative  $H_s$  (e.g., Bond and Fleagle, 1988). The latent heat flux ( $H_l$ ) also decreases within the warm sector as the specific humidity increases (Fig. 5c). However, in contrast to  $H_s$ ,  $H_l$  remains positive. The maximum  $H_l$  occurs just before the onset of the warm sector and at the very end of the post-frontal regime.

The covariance stress components can be used to compute a stress direction. If the stress is due entirely to wind waves, then the stress direction should be the same as the wind direction. If other factors, such as the swell, are influencing the stress, then the stress direction should be between the swell and wind direction. The composite of the difference between the stress and wind directions show that in the warm sector, the stress is usually greater than the wind direction by 5-12° (that is, the stress direction is to the right of the wind direction), while in the post-frontal regime the opposite appears to be true (Fig. 5d). Occasional manual observations of the swell direction by the ship's crew on the bridge show that the warm sector stress direction is frequently

between the swell direction and the wind direction (Fig. 6). These results suggest that in the vicinity of fronts, the stress vector may not be an accurate indicator of the wind direction. This has significant implications for remote sensing of surface winds over the oceans, and the use of such winds in diagnosing storm dynamics.

Inertial dissipation (ID) calculations of the surface fluxes also show the same qualitative trends that was noted for the covariance fluxes (Fig. 7a). However, the inertial dissipation stresses are slightly smaller than the covariance stresses, especially in the higher wind speed regime in the vicinity of the fronts. Furthermore, the ID sensible heat fluxes are lower near the fronts and higher in other areas. The differences in  $H_l$  are not quite as systematic, though there is still a tendency for the ID  $H_l$  to be weaker in the vicinity of the front.

The bulk fluxes (Fig. 8) calculated from the measured basic parameters and the bulk relationships of Fairall et al (2002) show the same general characteristics as discussed for the covariance and ID fluxes. However, the differences plot shows that the bulk stresses are

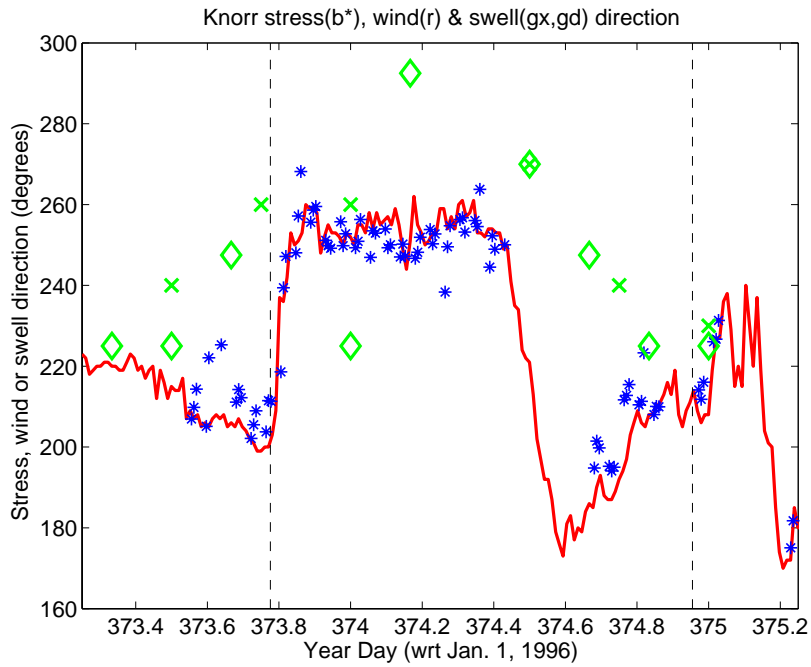


Fig. 6: Time series of wind direction from the R/V Knorr (red line), stress direction (blue\*), and manual observations of the swell direction from the ship's crew (green diamond, green "x"). The two vertical dashed lines show the frontal passages for cases 3 and 4.

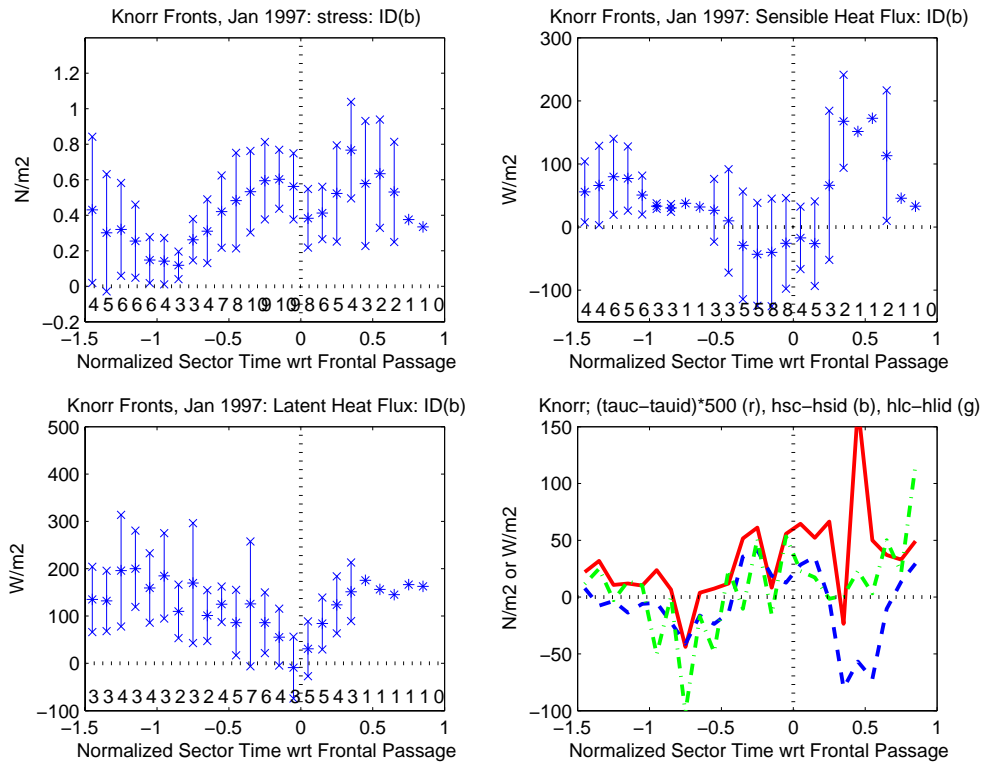


Fig. 7: Same as Fig. 5, but for fluxes calculated from the inertial dissipation technique. Panel d) shows the differences in the fluxes between the covariance and the inertial dissipation techniques. Note that the stress differences have been multiplied by 500 to scale properly on the plot.

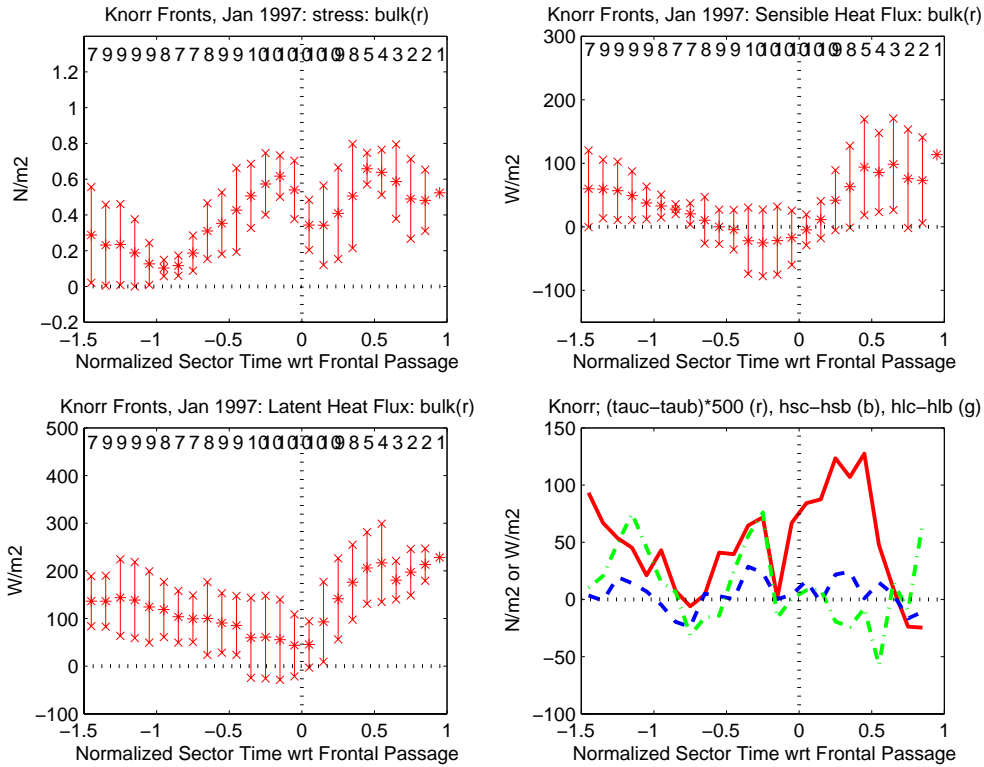


Fig. 8: Composites of a) stress, b) sensible heat flux, c) latent heat flux calculated from the bulk formulas of Fairall et al. (2002). In d), the differences between the covariance and bulk values of stress (red),  $H_s$  (blue) and  $H_l$  (green) are shown. Note that the stress differences have been multiplied by 500 to scale properly on the plot.

substantially (up to  $0.25 \text{ Nm}^{-2}$ ) smaller than the covariance ones, particularly in the post-frontal regime, and that the bulk  $H_s$  are  $10\text{-}20 \text{ Wm}^{-2}$  less than the covariance ones, especially in the vicinity of the fronts. The bulk  $H_l$  appear to be larger in the warm sector and smaller in the post-frontal regime. The reasons for the differences between the covariance, inertial dissipation, and the bulk fluxes are currently under investigation. These reasons may include real differences due to the assumptions inherent in the inertial dissipation and bulk techniques, and the effects of the wave conditions in the vicinity of the fronts.

## 5. CONCLUSIONS

Composites of atmospheric surface layer measurements were computed along ship paths through 10 storms in the North Atlantic Ocean. These composites show that:

a) The momentum flux is a maximum just before the frontal passage during the peak in wind speed associated with the warm-sector low-level jet. A second stress maximum of comparable magnitude occurs in the middle of the post-frontal regime for

the data from the *R/V Knorr* but not from the *Suroit*.

b) The latent and sensible heat fluxes are a minimum just before the frontal passage. Despite the strong surface winds at this time, the moistening and warming associated with synoptic-scale advective patterns and surface-layer fluxes minimize the vertical gradients in specific humidity and temperature. This pattern should affect the surface potential vorticity generation, and has dynamical implications for frontal stability.

c) Wave heights increase steadily from the eastern half of the warm sector to at frontal passage, remaining high through most of the post-frontal regime before decreasing.

d) Differences between covariance and inertial dissipation fluxes are largest during the times bracketing the cold front when the wave heights of the waves with period 6-9s are large and the covariance fluxes are large, and

e) the stress direction is consistently  $5\text{-}12^\circ$  to the right of the wind direction in the warm sector and  $2\text{-}15^\circ$  degrees to the left of the wind direction in the post-frontal regime. This last result implies

that satellite-based scatterometer wind directions, which rely on the surface stress field, will underestimate the surface directional wind shift across the front.

## 6. REFERENCES

- Bond, N. A., and R. G. Fleagle, 1988: Prefrontal and postfrontal boundary layer processes over the ocean, *Mon. Wea. Rev.*, **116**, 1257-1273.
- Fairall, C. W., A. B. White, J. B. Edson, and J. E. Hare, 1997: Integrated shipboard measurements of the marine boundary layer. *J. Atmos. Oceanic Technol.*, **14**, 338-359.
- Fairall, C. W., E. F. Bradley, J. E. Hare, A. A. Grachev, and J. B. Edson, 2002: Bulk parameterization of air-sea fluxes: Updates and verification for the COARE algorithm. *J. Clim.* Submitted.
- Joly, A., K. A. Browning, P. Bessemoulin, J.-P. Cammas, G. Caniaux, J.-P. Chalon, S. A. Clough, R. Dirks, K. A. Emanuel, L. Eymard, R. Gall, T. Hewson, P. H. Hildebrand, D. Jorgensen, F. Lalaurette, R. H. Langland, Y. Lemaître, P. Mascart, J. A. Moore, P. O. G. Persson, F. Roux, M. A. Shapiro, C. Snyder, Z. Toth, and R. Wakimoto, 1999: Overview of the field phase of the Fronts and Atlantic Storm-Track Experiment (FASTEX) project. *Quart. J. Roy. Meteor. Soc.*, **125**, 3131-3163
- Rieder, K. F., and J. A. Smith, 1998: Removing wave effects from the wind stress vector. *J. Geophys. Res.*, **103**, C1, 1363-1374.